Electronic Supplementary Information

Efficient ternary non-fullerene polymer solar cells with PCE of 11.92% and FF of 76.5%

Miao Zhang,[a] Wei Gao,[b] Fujun Zhang,*[a] Yang Mi,[c] Wenbin Wang,[a] Qiaoshi An,[a] Jian Wang,[d] Xiaoling Ma,[a] Jianli Miao,[a] Zhenghao Hu,[a] Xinfeng Liu,[c] Jian Zhang[e] and Chuluo Yang*[b]

Experimental section

Device Fabrication: All PSCs were fabricated with a conventional architecture of ITO/PEDOT:PSS/active layers/PDIN/Al. The patterned indium tin oxide (ITO) substrates with a sheet resistance of 15 Ω/□ were pre-cleaned by sequential ultrasonic treatment in detergent, deionized water and ethanol, respectively. The cleaned ITO substrates were further dried by high purity nitrogen and treated by oxygen plasma for 1 min to improve its work function and clearance. Poly(3,4-ethylenedioxythiophene):poly (styrene sulfonate) (PEDOT:PSS, clevios PVP Al 4083, purchased from H.C. Starck Co., Ltd.) solution was spin-coated on the ITO substrates at 5000 round per minute (RPM) for 40 s and then baked at 150℃ for 15 min in air. The used PDIN and PBDB-T were purchased from Solarmer Materials Inc. and the acceptors of ITCPTC, IDT6CN-M were synthesised by Yang's group from department of chemistry, Wuhan University. The PBDB-T:ITCPTC and PBDB-T:IDT6CN-M with 1:1.2 weight ratio were dissolved in chlorobenzene (adding 0.3% v/v of 1,8-diiodooctane, DIO) to prepare 18 mg/mL binary blend solutions, respectively. After heated and stirred at 40℃ about 3 h, binary blend solutions were mixed by different volume ratios to obtain ternary blend solutions of PBDB-T_{100}:IDT6CN-M_{100-x}:$ITCPTC_x$ (x=0, 10, 20, 30, 40, 50, 60, 70, 80, 90, 100 wt%, x represents ITCPTC content in acceptors). Subsequently, the prepared blend solutions were spin-coated on PEDOT:PSS modified ITO substrates at 2500 RPM for 40 s in high-purity nitrogen-filled glove box. Then the active layers were annealed at 120℃ for 5min. The methanol solution (0.3% acetic acid) of PDIN at a concentration of 2 mg/mL was spin-coated onto active layers at 5000 RPM for 40 s to prepare cathode interlayer. Finally, 100 nm Al was deposited by thermal evaporation with a shadow mask. The effective area of cell is 3.8 mm^2, which is defined by the vertical overlap of ITO anode and Al cathode.

Device Measurement: Current-voltage (*I-V*) curves of PSCs were measured using a Keithley 2400 source meter in high-purity nitrogen-filled glove box. The AM 1.5 illumination was provided by a XES-40S2-CE (SAN-EI Electric Co., Ltd.) solar simulator (AAA class, 40×40 mm^2 effective irradiated area) with light

intensity of 100 mW/cm^2. This light intensity was calibrated by standard silicon solar cells purchased from Zolix INSTRUMENTS CO., LTD. The different light intensity was obtained by a set of neutral optical filters with transmission of 10%, 25%, 50% and 79%, respectively. External quantum efficiency (EQE) spectra of PSCs were measured by a Zolix Solar Cell Scan 100. The optimized thickness of active layers was ~120 nm measured by an Ambios Technology XP -2 stylus Profiler. Absorption spectra of films were obtained by a Shimadzu UV-3101PC spectrometer. Photoluminescence (PL) spectra of films were measured by a HORIBA Fluorologs-3 spectrofluorometer system. Femtosecond transient absorption spectra (TAS) measurement was performed using a commercial fs-TAS system, i.e., HELIOS (Ultrafast Systems). The 800 nm pulses from a Coherent Astrella regenerative amplifier (80 fs, 1 kHz, 2.5 mJ/pulse), seeded by a Coherent Vitara-s oscillator (35 fs, 80 MHz), was used to pump an optical parametric amplifier (Coherent, OperA Solo) to generate excitation pulse at 400 nm. The pump beam was chopped at 500 Hz with pump fluence at ~ 20 μJ/cm^2, while a small fraction of the 800 nm output from the Astrella was fed to a sapphire crystal in the HELIOS for generating the white light continuum (WLC). A 750 nm short pass filter (SPF) is typically used to suppress the residual 800 nm from the WLC generation. The system has an ultimate temporal resolution of ~130 fs. The lifetimes were fitted using a Gaussian response function convoluted with a triple exponential decay function:

$$\Delta A(t) = A + B_1 exp\left(\frac{-t}{\tau_1}\right) + B_2 exp\left(\frac{-t}{\tau_2}\right) + B_3 exp\left(\frac{-t}{\tau_3}\right)$$

A is value for the background and B are the values for amplitude fit parameters. Cyclic voltammetry (CV) measurements were carried out on a CHI voltammetric analyzer at room temperature. Tetrabuty-lammonium hexafluorophosphate (n-Bu4NPF6, 0.1 M) was used as the supporting electrolyte. The conventional three-electrode configuration consists of a platinum working electrode with a 2 mm diameter, a platinum wire counter electrode, and a Ag/AgCl wire reference electrode. Cyclic voltammograms were obtained at a scan rate of 100 mV s^{-1}. The potentials were determined using ferrocene as the reference. The HOMO and LUMO energy levels were calculated according to the following equations:

$$HOMO = -\left[E_{ox} + \left(4.80 - E_{Fc}\right)\right] eV;$$

$$LUMO = -\left[E_{red} + \left(4.80 - E_{Fc}\right)\right] eV;$$

where E_{ox} and E_{red} are the onset of oxidation and reduction potential, respectively. Transmission electron microscopy (TEM) images of the active layers were obtained by using a JEOL JEM-1400 transmission electron microscope operated at 80 kV. The grazing incidence x-ray diffraction (GIXD) data were obtained at 1W1A, Beijing Synchrotron Radiation Facility (BSRF). A bent-triangle silicon crystal was used to select the X-rays of a 1.5476 Å wavelength and an optimal grazing angle of 0.2° was selected to maximum the diffraction peak intensity from the samples. The hole and electron mobility were calculated according to the space charge limited current (SCLC) method. The charge mobility is generally described by the Mott-Gurney equation:

$$J = \frac{9}{8}\varepsilon_0\varepsilon_r\mu\frac{V^2}{L^3}$$

Where J is the current density, ε_0 is the permittivity of free space (8.85×10^{-14} F/cm), ε_r is the dielectric constant of used materials which is assumed to be 3, a typical value for organic materials, μ is the charge mobility, V is the applied voltage and L is the active layer thickness.

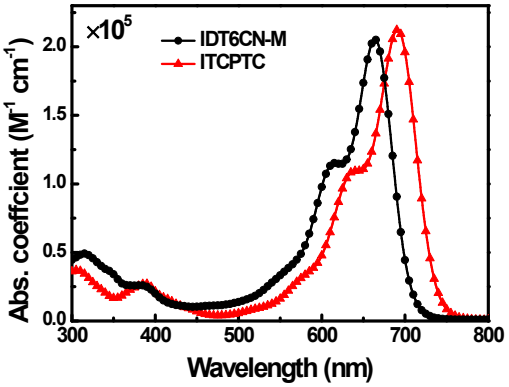

Fig. S1 Molar extinction coefficient spectra of IDT6CN-M and ITCPTC in dilute chloroform solution (10^{-5} M).

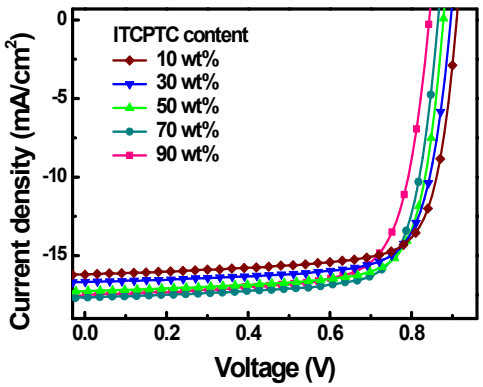

Fig. S2 *J-V* characteristics of ternary PSCs with different ITCPTC content in acceptors.

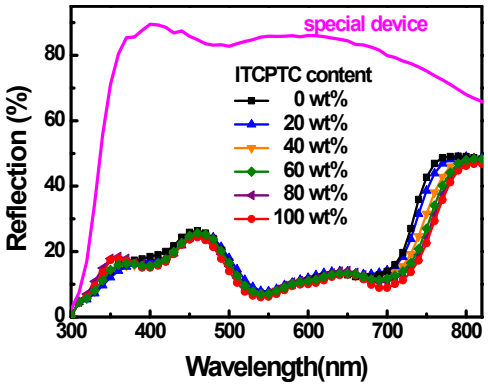

Fig. S3 The reflection spectra of PSCs with different ITCPTC content in acceptors and a special device ITO/PEDOT:PSS/PMMA (~120 nm)/PDIN/Al.

The reflection measurement of all devices was performed on a commercial QE measurement system (QE-RT3011, Enlitech) by using an integrating sphere. The absorption spectra of active layers were calculated by subtracting the parasitic absorptions (1-R_1) from the total absorption in PSCs (1-R_2), where R_1 is the reflection spectrum of device ITO/PEDOT:PSS/PMMA (~120 nm)/PDIN/Al, R_2 is the reflection spectra of PSCs ITO/PEDOT:PSS/active layers (~120 nm)/PDIN/Al. The PMMA layer is used to simulate the interference effect between incident light and reflected light from Al electrode in the active layers because PMMA has negligible absorption in the whole spectral range.

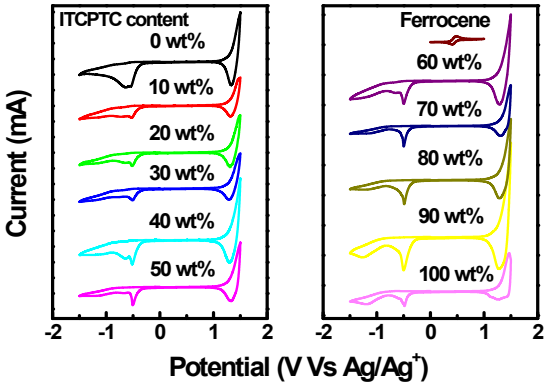

Fig. S4 Cyclic voltammetry (CV) plots of ITCPTC:IDT6CN-M blend films with different ITCPTC content.

Table S1. The E_{red}, E_{ox}, HOMO and LUMO energy levels of blend films with different ITCPTC content extracted from the corresponding CV curves.

ITCPTC content	E_{red} (V)	E_{ox} (V)	LUMO (eV)	HOMO (eV)
0 wt %	-0.4372	1.3200	-3.9203	-5.6775
10 wt %	-0.4311	1.3188	-3.9264	-5.6763

20 wt %	-0.4268	1.3167	-3.9307	-5.6742
30 wt %	-0.4202	1.3132	-3.9373	-5.6706
40 wt %	-0.4123	1.3114	-3.9452	-5.6689
50 wt %	-0.4064	1.3080	-3.9511	-5.6655
60 wt %	-0.4034	1.3063	-3.9541	-5.6638
70 wt %	-0.3996	1.3032	-3.9579	-5.6607
80 wt %	-0.3924	1.2951	-3.9651	-5.6526
90 wt %	-0.3872	1.2894	-3.9703	-5.6469
100 wt%	-0.3811	1.2831	-3.9764	-5.6406

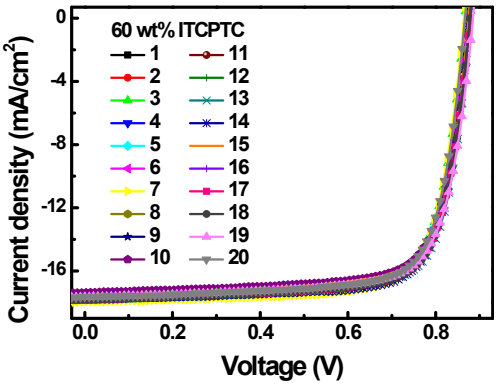

Fig. S5 *J-V* characteristics of the twenty optimized ternary PSCs prepared from different batches under AM 1.5G illumination with light intensity of 100 mW/cm^2.

Table S2. Photovoltaic parameters of the twenty optimized ternary PSCs prepared from different batches.

Devices	J_{SC} [mA/cm^2]	V_{OC} [V]	FF [%]	PCE [%]
1	17.45	0.873	76.5	11.65
2	17.75	0.875	75.6	11.74
3	17.57	0.868	76.0	11.59
4	17.52	0.872	76.4	11.67
5	17.65	0.873	75.6	11.65
6	17.63	0.874	76.1	11.73
7	17.95	0.867	75.8	11.79
8	17.68	0.870	75.8	11.66
9	17.58	0.878	76.0	11.72
10	17.37	0.873	75.8	11.49
11	17.69	0.872	76.5	11.80
12	17.59	0.875	76.0	11.69
13	17.81	0.880	76.1	11.93
14	17.81	0.875	76.5	11.92
15	17.59	0.871	75.5	11.57
16	17.59	0.873	76.1	11.69
17	17.84	0.875	75.8	11.83

18	17.79	0.878	75.9	11.85
19	17.64	0.880	75.6	11.74
20	17.65	0.870	75.5	11.60

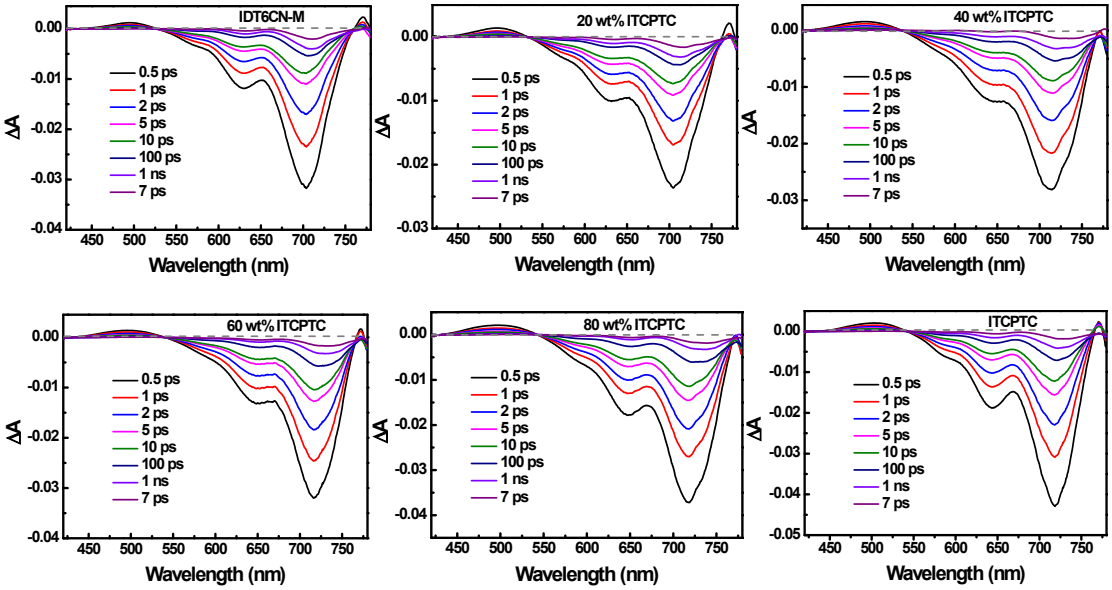

Fig. S6 Transient absorption spectra of ITCPTC:IDT6CN-M blend films with different ITCPTC content under 400 nm light excitation.

Table S3. The fitted lifetime of 750 nm of acceptor blend films with different ITCPTC content.

ITCPTC content	τ_1 (ps)	τ_2 (ps)	τ_3 (ps)
20 wt%	2.21±0.04 (66.4%)	55.2±5.1 (4.4%)	2364±46 (21.2%)
40 wt%	1.74±0.03 (65.5%)	52.4±4.8 (8.4%)	2026±46 (26.1%)
60 wt%	1.46±0.02 (64.9%)	49.8±3.6 (11.4%)	1950±48 (23.7%)
80 wt%	1.23±0.02 (67.8%)	45.1±2.9 (11.6%)	1825±52 (20.6%)
100 wt%	1.03±0.02 (69.9%)	30.0±0.2 (10.2%)	1782±46 (19.9%)

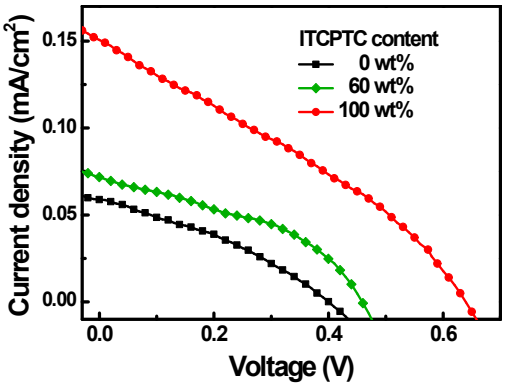

Fig. S7 *J-V* curves of devices with IDT6CN-M, ITCPTC:IDT6CN-M (60 wt% ITCPTC) or ITCPTC as active layers under AM 1.5G illumination with light intensity of 100 mW/cm^2.

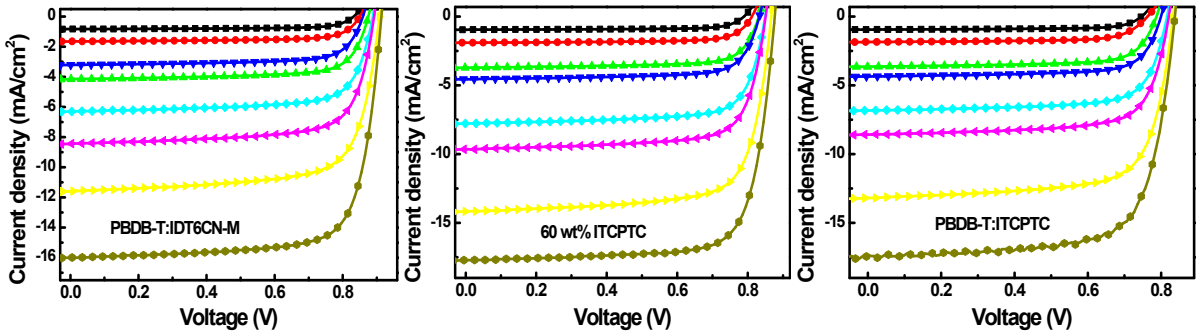

Fig. S8 *J-V* curves of binary and the optimized ternary PSCs under under AM 1.5G illumination with light intensity of 100, 79, 50, 39.5, 25, 19.8, 10, 5 mW/cm^2, respectively.

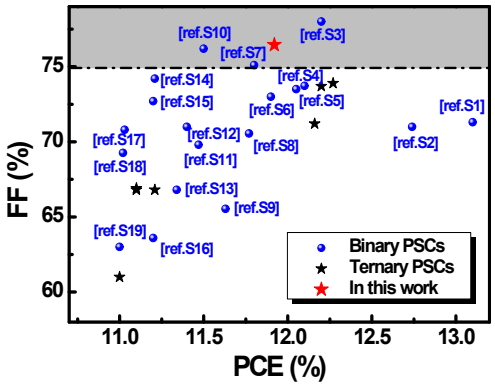

Fig. S9 The FF values of efficient binary and ternary PSCs with PCE over 11%.

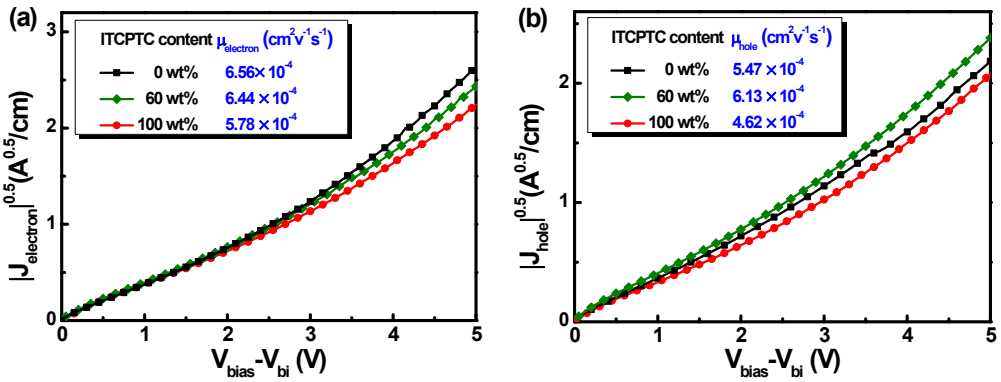

Fig. S10 $J^{0.5}$-*V* curves of (a) electron-only and (b) hole-only devices with the corresponding active layers in dark.

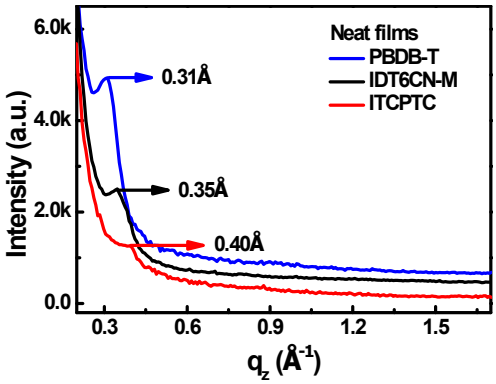

Fig. S11 The OOP line-cuts of neat PBDB-T, IDT6CN-M and ITCPTC films.

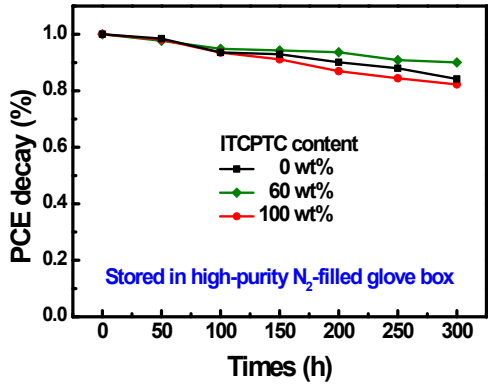

Fig. S12 Stability of binary PSCs and the optimized ternary PSCs after 300 h storage in high-purity N_2-filled glove box.

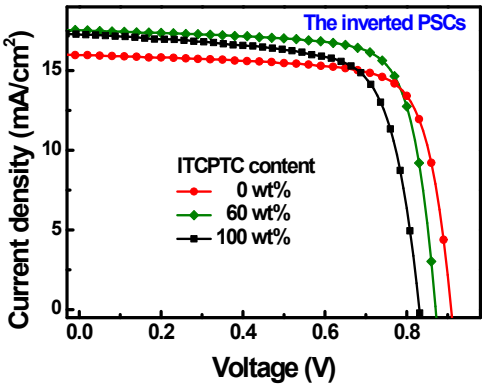

Fig. S13 *J-V* curves of binary PSCs and the optimized ternary inverted PSCs with a structure of ITO/ZnO/Active layer/MoO_3/Ag under AM 1.5G illumination with light intensity of 100 mW/cm^2.

Table S4 Photovoltaic parameters of binary and the optimized ternary inverted PSCs.

ITCPTC content	J_{SC} [mA/cm^2]	V_{OC} [V]	FF [%]	PCE [%]
0 wt%	15.97	0.910	75.18	10.93
60 wt%	17.54	0.871	75.82	11.58
100 wt%	17.26	0.829	71.21	10.19

References

1 W. Zhao, S. Li, H. Yao, S. Zhang, Y. Zhang, B. Yang and J. Hou, *J. Am. Chem. Soc.*, 2017, **139**, 7148-7151.

2 S. j. Xu, Z. Zhou, W. Liu, Z. Zhang, F. Liu, H. Yan and X. Zhu, *Adv. Mater.*, 2017, **29**, 11704510.

3 S. Li, L. Ye, W. Zhao, X. Liu, J. Zhu, H. Ade and J. Hou, *Adv. Mater.*, 2017, **29**, 1704051.

4 F. Zhao, S. Dai, Y. Wu, Q. Zhang, J. Wang, L. Jiang, Q. Ling, Z. Wei, W. Ma, W. You, C. Wang and X. Zhan, *Adv. Mater.*, 2017, **29**, 1700144.

5 S. Li, L. Ye, W. Zhao, S. Zhang, S. Mukherjee, H. Ade and J. Hou, *Adv. Mater.*, 2016, **28**, 9423-9429.

6 S. Li, L. Ye, W. Zhao, S. Zhang, H. Ade and J. Hou, *Adv. Energy Mater.*, 2017, **7**, 1700183.

7 D. Xie, T. Liu, W. Gao, C. Zhong, L. Huo, Z. Luo, K. Wu, W. Xiong, F. Liu, Y. Sun and C. Yang, *Solar RRL*, 2017, **1**, 1700044.

8 Y. Yang, Z.-G. Zhang, H. Bin, S. Chen, L. Gao, L. Xue, C. Yang and Y. Li, *J. Am. Chem. Soc.*, 2016, **138**, 15011-15018.

9 L. Xue, Y. Yang, J. Xu, C. Zhang, H. Bin, Z.-G. Zhang, B. Qiu, X. Li, C. Sun, L. Gao, J. Yao, X. Chen, Y. Yang, M. Xiao and Y. Li, *Adv. Mater.*, 2017, **29**, 1703344.

10 B. Guo, W. Li, X. Guo, X. Meng, W. Ma, M. Zhang and Y. Li, *Adv. Mater.*, 2017, **29**, 1702291.

11 T. Yu, X. Xu, G. Zhang, J. Wan, Y. Li and Q. Peng, *Adv. Funct. Mater.*, 2017, **27**, 1701491.

12 H. Yao, L. Ye, J. Hou, B. Jang, G. Han, Y. Cui, G. M. Su, C. Wang, B. Gao, R. Yu, H. Zhang, Y. Yi, H. Y. Woo, H. Ade and J. Hou, *Adv. Mater.*, 2017, **29**, 1700254.

13 Z. Zheng, O. M. Awartani, B. Gautam, D. Liu, Y. Qin, W. Li, A. Bataller, K. Gundogdu, H. Ade and J. Hou, *Adv. Mater.*, 2017, **29**, 1604241.

14 W. Zhao, D. Qian, S. Zhang, S. Li, O. Inganäs, F. Gao and J. Hou, *Adv. Mater.*, 2016, **28**, 4734-4739.

15 H. Feng, N. Qiu, X. Wang, Y. Wang, B. Kan, X. Wan, M. Zhang, A. Xia, C. Li, F. Liu, H. Zhang and Y. Chen, *Chem. Mater.*, 2017, **29**, 7908-7917.

16 S. Chen, Y. Liu, L. Zhang, P. C. Y. Chow, Z. Wang, G. Zhang, W. Ma and H. Yan, *J. Am. Chem. Soc.*, 2017, **139**, 6298-6301.

17 Y. Lin, F. Zhao, Y. Wu, K. Chen, Y. Xia, G. Li, S. K. K. Prasad, J. Zhu, L. Huo, H. Bin, Z.-G. Zhang, X. Guo, M. Zhang, Y. Sun, F. Gao, Z. Wei, W. Ma, C. Wang, J. Hodgkiss, Z. Bo, O. Inganäs, Y. Li and X. Zhan, *Adv. Mater.*, 2017, **29**, 1604155.

18 S. Chen, H. J. Cho, J. Lee, Y. Yang, Z.-G. Zhang, Y. Li and C. Yang, *Adv Energy Mater*, 2017, **7**, 1701125.

19 J. Wang, W. Wang, X. Wang, Y. Wu, Q. Zhang, C. Yan, W. Ma, W. You and X. Zhan, *Adv. Mater.*, 2017, **29**, 1702125.